PAPER

Perpendicular magnetic anisotropy in half-metallic thin-film Co₂CrAl

To cite this article: Ryan Carlile et al 2021 J. Phys.: Condens. Matter 33 105801

View the <u>article online</u> for updates and enhancements.



IOP ebooks™

Bringing together innovative digital publishing with leading authors from the global scientific community.

Start exploring the collection-download the first chapter of every title for free.

J. Phys.: Condens. Matter 33 (2021) 105801 (7pp)

https://doi.org/10.1088/1361-648X/abd052

Perpendicular magnetic anisotropy in half-metallic thin-film Co₂CrAl

Ryan Carlile¹, Juliana Herran^{2,3}, Shashi Poddar⁴, Eric J Montgomery⁴, Parashu Kharel⁵, Paul M Shand¹ and Pavel V Lukashev^{1,*}

- ¹ Department of Physics, University of Northern Iowa, Cedar Falls, IA 50614, United States of America
- ² Department of Chemistry and Biochemistry, University of Northern Iowa, Cedar Falls, IA 50614, United States of America
- ³ Université de Franche-Comté, 25000 Besançon, France
- ⁴ Euclid BeamLabs, Bolingbrook, IL 60440, United States of America
- ⁵ Department of Physics, South Dakota State University, Brookings, SD 57007, United States of America

E-mail: pavel.lukashev@uni.edu

Received 24 October 2020, revised 16 November 2020 Accepted for publication 3 December 2020 Published 23 December 2020



Abstract

Magnetocrystalline anisotropy (MCA) is one of the key parameters investigated in spin-based electronics (spintronics), e.g. for memory applications. Here, we employ first-principles calculations to study MCA in thin film full Heusler alloy Co₂CrAl. This material was studied in the past, and has been reported to exhibit half-metallic electronic structure in bulk geometry. In our recent work, we showed that it retains a 100% spin-polarization in thin-film geometry, at CrAl atomic surface termination. Here, we show that the same termination results in a perpendicular magnetic anisotropy, while Co surface termination not only destroys the half-metallicity, but also results in in-plane magnetization orientation. In addition, for films thicker than around 20 nm the contribution from magnetic shape anisotropy may become decisive, resulting in in-plane magnetization orientation. To the best of our knowledge, this is one of the first reports of half-metallic thin-film *surfaces* with perpendicular magnetic anisotropy. This result may be of interest for potential nano-device applications, and may stimulate a further experimental study of this and similar materials.

Keywords: perpendicular magnetic anisotropy, half-metals, Heusler alloys, spintronics (Some figures may appear in colour only in the online journal)

1. Introduction

Magnetocrystalline anisotropy in magnetic thin films is one of the most important parameters for applications in modern spin-based electronics, e.g. for magnetic data storage [1–6]. In particular, MCA determines the orientation of magnetization direction, and thermal stability of magnetic materials. Perpendicular magnetic anisotropy (PMA) in thin films has attracted particular attention for various device applications, such as spin-transfer torque driven magnetization switching in magnetoresistive random-access memory [7–9]. In addition to magnetic field, various mechanisms have been suggested to

manipulate and control the magnetic anisotropy, such as electric field [10–13], mechanical strain [14, 15], applied voltage [16–19], and ferroelectric switching [20, 21].

Among other materials that have been investigated for PMA applications, Heusler alloys attracted particular attention, in part due to their high Curie temperature, and relative ease of fabrication. In particular, PMA has been reported in thin-film Co₂FeAl and Co₂FeSi grown on MgO [22, 23]. In addition to potentially exhibiting surface/interface PMA, Heusler compounds have been extensively studied as halfmetals, i.e. materials that are conducting for one spin channel, while insulating/semiconducting for the opposite spin channel, which makes them 100% spin-polarized. In recent years, many Heusler alloys have been suggested to exhibit a

^{*} Author to whom any correspondence should be addressed.

100% spin-polarization (SP), both experimentally and theoretically [24–32]. For practical applications, combining PMA with half-metallicity in thin-film geometry could provide additional functionalities for spintronic devices. To the best of our knowledge, this topic has not received sufficient attention so far in the literature. In this paper, we address this issue by performing a computational study of thin-film Co₂CrAl. It will be demonstrated that at CrAl surface termination, this material may exhibit a robust PMA along with 100% SP.

The full Heusler compound Co₂CrAl has been extensively studied in the past, both experimentally and theoretically. The first report dates back to early 1980s, when Buschow and Engen showed that Co₂CrAl crystallizes in cubic L2₁ structure, with ferromagnetic alignment, and a Curie temperature of 334 K [33]. This followed by a series of papers, which, among other things, reported a half-metallic electronic structure of this compound [34–40]. The magnetocrystalline anisotropy of polycrystalline Co₂CrAl sample was experimentally studied by Kourov et al [41]. In particular, they estimated the MCA energy of the alloy as $\sim 5 \times 10^5$ erg g⁻¹. In addition, the transport properties of this material have been studied by many groups, mainly reporting the dependence of resistivity on atomic disorder [42, 43]. We have also presented a somewhat extensive literature overview of this material in our recent publication, see reference [31].

In our recent work [31], we showed that Co_2CrAl retains a 100% SP in thin-film geometry at CrAl surface termination, while half-metallicity is destroyed at Co surface termination due to the emergence of minority-spin surface states at the Fermi level. In addition, the half-metallic electronic structure of CrAl surface is retained for a wide range of both uniform pressure and biaxial strain. These properties make this material very attractive for potential device applications. The purpose of the current work is to analyze the MCA in thin-film Co_2CrAl , at both CrAl and Co surface terminations. It will be shown that the CrAl termination not only results in a robust half-metallicity, but also exhibits the PMA, unlike the Co termination, which lacks both properties.

The rest of the paper is organized as follows. In section 2, we outline the computational methods and techniques. Section 3 presents our main results, and consists of three subsections—the first sub-section presents a brief overview of electronic, magnetic, and structural properties of Co₂CrAl, the second sub-section is focused on MCA energy calculations at equilibrium lattice parameters, while the third subsections shows the response of MCA to external pressure and strain. Section 4 contains a brief discussion for practical implementations and a summary of this work, followed by acknowledgments and references.

2. Computational methods and techniques

We perform density functional calculations of thin-film Co₂CrAl full Heusler alloy, using the projector augmented-wave method (PAW) [44], implemented in the Vienna *ab initio* simulation package [45] within the generalized-gradient approximation [46]. The integration method [47] with a 0.05 eV width of smearing is used. The cut-off energy of the

plane-waves is set to 500 eV. Structural optimization is performed with the energy convergence criteria of 10^{-2} meV, which results in the Hellmann–Feynman forces being less than 0.005 eV Å $^{-1}$. The total energy and electronic structure calculations are performed with a stricter convergence criteria of 10^{-3} meV. The Brillouin zone integration is performed with a k-point mesh of $16 \times 16 \times 1$. Some of the results and figures (such as the crystal structure visualization) are obtained using the MedeA $^{(8)}$ software environment [48]. Most of the calculations are performed using Extreme Science and Engineering Discovery Environment (XSEDE) resources located at the Pittsburgh Supercomputing Center (PSC) [49], and the resources of the Center for Functional Nanomaterials (CFN) at Brookhaven National Laboratory (BNL).

The thin-film calculations are performed on a 64-atom stoichiometric super-cell (four 16-atom unit cells stacked in (001) direction) with asymmetrically terminated surfaces. A 20 Å vacuum layer is imposed to avoid the overlap of the surface wave functions. Periodic boundary condition is imposed for all calculations.

The magnetocrystalline anisotropy energy (MAE) is estimated as the difference of total energies calculated self-consistently for the magnetization pointing along the x and z directions (MAE = $E_x - E_z$) in the presence of spin-orbit coupling (SOC). Thus, a positive MAE indicates out-of-plane magnetization orientation, i.e. PMA, while a negative MAE indicates in-plane magnetization. The convergence of MAE with respect to the k-mesh was thoroughly tested, and a good convergence was achieved at the k-mesh of $16 \times 16 \times 1$, which was used to calculate the results presented below.

The site-projected contributions to MAE are calculated by evaluating the expectation values for the SOC energies: $E_{\text{SOC}} = \langle \frac{\hbar^2}{2m^2c^2} \frac{1}{r} \frac{\mathrm{d}V}{\mathrm{d}r} L S \rangle$, where r is the distance in each atomic sphere, V is the spherical part of the effective potential as a function of r, and L and S are orbital and spin operators, respectively [50, 51]. These expectation values are twice the actual values of the total energy correction to the second order in SOC [6, 52].

3. Results

3.1. Electronic, magnetic, and crystal structures

The full Heusler compound, Co_2CrAl crystallizes in $L2_1$ structure (see figure 1(c)), with equilibrium lattice parameter of 5.728 Å, and is half-metallic in bulk geometry, with the minority-spin band gap of 0.470 eV. The magnetic alignment is ferromagnetic, with 3.00 μ_B/f .u. ($\approx 0.75~\mu_B/Co$ and $\approx 1.55~\mu_B/Cr$). The integer magnetic moment per formula unit is consistent with half-metallicity, as all minority-spin states in the valence band are occupied, which makes their total number an integer, resulting in an integer total magnetic moment, because of the integer total valence charge. See reference [31], and references therein for a more detailed discussion of the bulk properties of Co_2CrAl .

In our recent work, we showed that Co₂CrAl exhibits ground state half-metallicity in thin-film geometry, at CrAl surface termination, while Co-termination results in reduced

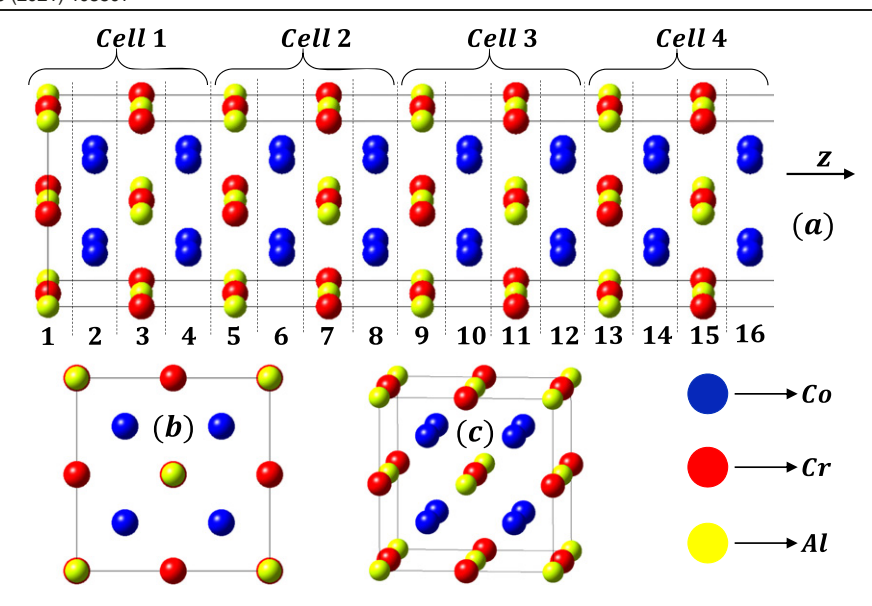


Figure 1. (a) 64-atom super-cell of thin-film Co_2CrAl ; (b) top view of the 64-atom super-cell; (c) unit cell of the bulk Co_2CrAl . Atoms are color coded as indicated in the figure. The out-of-plane z-direction is shown in the figure.

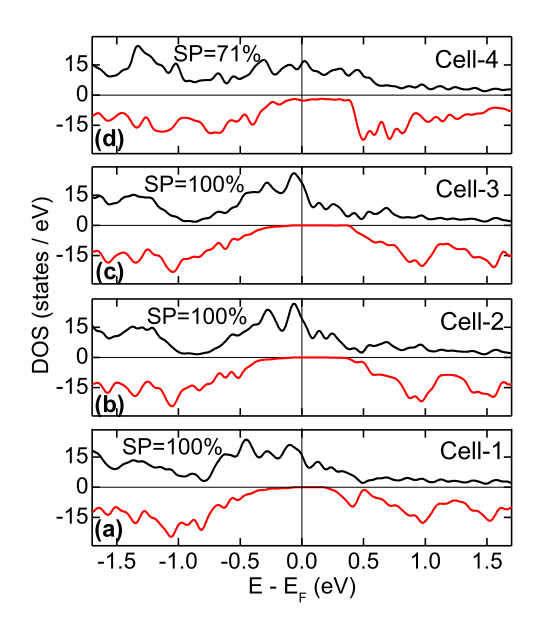


Figure 2. Cell-resolved DOS of thin-film Co₂CrAl for the 64-atom cell shown in figure 1(a). Vertical lines indicate the position of the Fermi level. Positive (black line) and negative (red line) DOS correspond to majority- and minority-spin states, correspondingly. The labeling of the cells is consistent with the one shown in figure 1(a). SP values of each cell are indicated in the figure.

SP, due to the emergence of minority-spin surface states at the Fermi level [31]. These results are summarized in figure 2, which shows the calculated cell-resolved density of states (DOS) for the 64-atom structure shown in figure 1(a). The labeling of the cells is consistent with the one shown in figure 1(a), in particular cells 1 and 4 represent the CrAl- and Co-terminated surfaces, correspondingly, while cells 2 and 3 possess a bulk-like symmetry, i.e. no termination surface. As one can see from figure 2, cells 2 and 3 exhibit a half-metallic bulk-like behavior (figures 2(b) and (c)), which is retained at

CrAl-terminated cell 1 (figure 2(a)). At the same time, the half-metallicity is destroyed at Co-terminated cell 4 (figure 2(d)), due to the emergence of minority-spin surface states around Fermi energy. It is to be noted that the optimized in-plane lattice constant of the 64-atom cell is 5.641 Å, i.e. slightly smaller than the corresponding equilibrium bulk value of 5.728 Å. For a more detailed discussion of the electronic structure of thin-film Co₂CrAl, see reference [31].

3.2. Calculated MAE at equilibrium lattice constant

Figure 3(a) shows calculated atom-resolved MAE of the 64-atom cell (see figure 1(a)) without structural optimization, at the bulk lattice parameter of 5.728 Å. MAE of Al atoms is negligible, and is not shown/discussed in the rest of the paper. Let us first look at the MAE of Co atoms (blue line and squares). There are 8 atomic layers (in z-direction) in the cell containing Co, and only one of them has a sizable MAE, namely the surface layer 16, with around -1.2 meV/Co. This contribution clearly comes from the surface MCA of cobalt, and its negative value serves as an indication of in-plane magnetization orientation. Now, let us look at the MAE of Cr atoms (red line and circles). There are 8 atomic layers containing Cr (in z-direction), and the main contribution to MAE comes from the leftmost and rightmost layers. In particular, the surface layer (numbered 1 in figure 1(a)) has a positive MAE of around 0.5 meV/Cr, thus indicating out-of-plane magnetization orientation. At the same time, at the layer 15, i.e. the one adjacent to the surface Co layer, the calculated MAE of Cr is negative (slightly under -0.4 meV/Cr by magnitude), indicating in-plane magnetization orientation. The negative MAE of Cr at the layer 15 probably comes from the orbital hybridization of Cr with the surface Co layer, which exhibits in-plane magnetization orientation.

Figure 3(b) shows layer-resolved MAE of the 64-atom cell (see figure 1(a)) without structural optimization. The numbering of the atomic layers is consistent with the one shown in

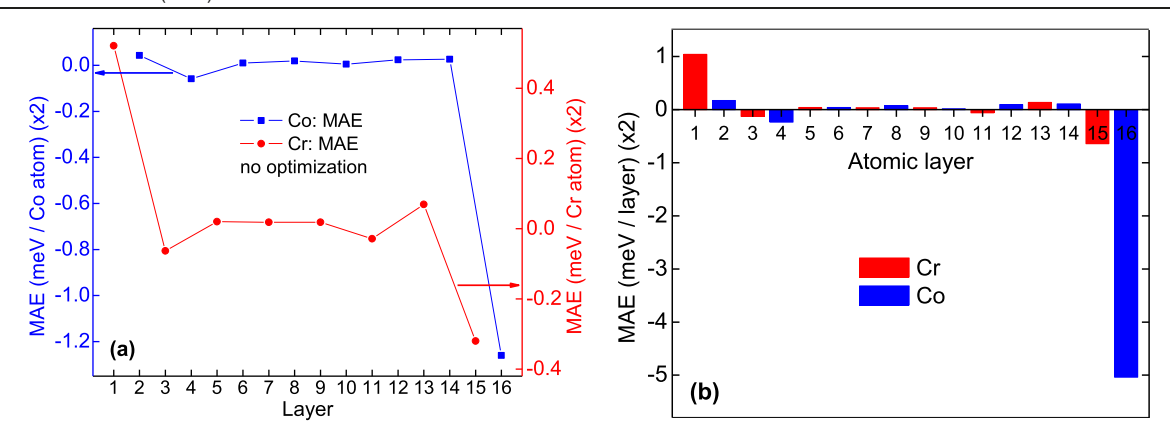


Figure 3. (a) Atom-resolved MAE, calculated without structural optimization. Blue line and squares—Co, red line and circles—Cr. (b) Layer-resolved MAE, calculated without structural optimization. Numbering of the atomic layers is consistent with the one shown in figure 1(a). Red columns—Cr layers, blue columns—Co layers. As explained in the computational methods section, the reported values are twice the actual values of the total energy correction to the second order in SOC.

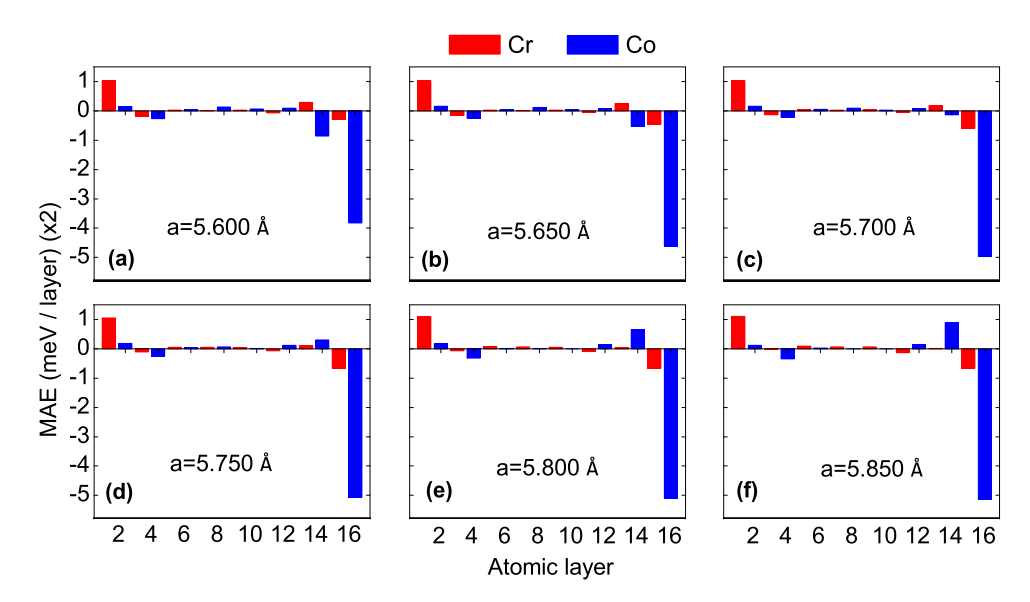


Figure 4. Layer-resolved MAE, calculated at different lattice constants (as indicated on the figure), without structural optimization, i.e. with the cubic symmetry retained. Numbering of the layers is consistent with the one shown in figure 1(a). Red columns—Cr layers, blue columns—Co layers. The reported values are twice the actual values of the total energy correction to the second order in SOC.

figure 1(a). Conceptually, although figures 3(a) and (b) contain similar information, figure 3(b) is mostly used for better visualization. The layer-resolved MAE shown in figure 3(b) is simply calculated by adding atom-resolved MAE contributions shown in figure 3(a), i.e. all Cr contributions are multiplied by 2, and all Co contributions are multiplied by 4, which are the numbers of these atoms per layer in our 64-atom supercell. Figure 3(b) clearly shows two surface MCAs, one with in-plane (Co surface) and one with out-of-plane (CrAl surface) magnetization orientations.

3.3. Calculated MAE under pressure and strain

In our recent work, we showed that the thin-film half-metallicity of Co₂CrAl is retained under a wide range of uniform pressure and biaxial strain [31]. In this sub-section, we look at the effect of pressure and strain on the calculated MCA energies of this compound.

Figure 4 shows layer-resolved MAE of the 64-atom cell (see figure 1(a)), calculated at different lattice constants (shown in the figure), without structural optimization, i.e. with the cubic symmetry retained. Qualitatively, these results are similar to the ones shown in figure 3(b), i.e. the in-plane magnetization orientation of the surface Co layer, and the out-ofplane magnetization orientation of the surface Cr layer are retained, while the 'bulk-like' layers have negligible contribution to MAE. The magnitude of the calculated surface MAE is also not very sensitive to the uniform pressure, except a small reduction of the surface Co MAE under uniform compression. At the same time, an interesting behavior of the layer 14 MAE (second Co layer from the right surface) should be noted. At the largest considered compression, it is negative, indicating in-plane magnetization orientation. But increasing the lattice parameter results in increase of the layer 14 MAE, i.e. it becomes less negative, and at around equilibrium

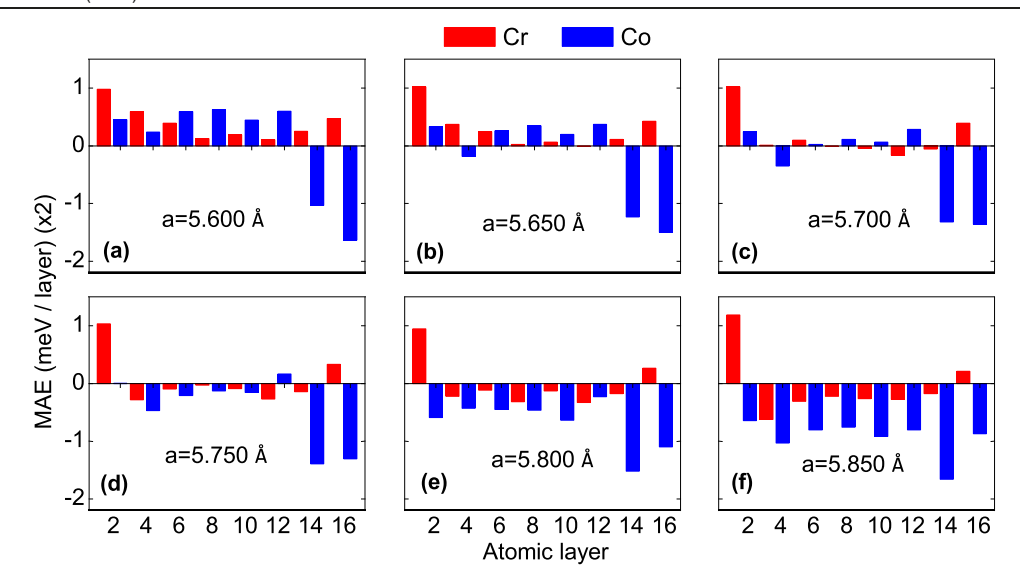


Figure 5. Layer-resolved MAE, calculated at different lattice constants under biaxial strain, with fixed in-plane lattice parameters (shown in the figure), and optimized out-of-plane coordinates. Numbering of the atomic layers is consistent with the one shown in figure 1(a). Red columns—Cr layers, blue columns—Co layers. The reported values are twice the actual values of the total energy correction to the second order in SOC.

lattice constant it changes sign and further increases with the uniform expansion of the cell. Although this result is not very significant for the main conclusions reported in this work, one possible mechanism responsible for this behavior could be the change of the hybridization strength between layers 14 and 16, under uniform pressure. In particular, under compression, the interlayer distances in *z*-direction are smaller, and the in-plane MCA of the layer 14 could be induced by its hybridization with the surface layer 16. This hybridization reduces as the volume of the cell increases, which may results in a change of the magnetization direction of the layer 14. Layers further from the surface do not exhibit any noticeable correlation with the volume of the cell, since they can be treated as having bulk-like properties of a cubic cell, i.e. negligible magnetic anisotropy.

While the (rather minimal) effect of the uniform pressure on MCA of Co₂CrAl may be an interesting observation, in actual experimental setup (e.g. in thin-film multilayers), a biaxial strain is a more realistic scenario. Therefore, next we analyze the effect of the epitaxial strain on the calculated MAE. This is done as follows. The in-plane lattice parameters are fixed at the same values as shown in figure 4, while the out-of-plane coordinates are optimized. Once the equilibrium geometry is obtained, MAE is calculated. The results are shown in figure 5.

The main physical consequence of biaxial strain is breaking of the cubic symmetry, induced by a tetragonal distortion. This results in a significant effect on MAE. In particular, as shown in figure 5, the calculated MAE of the surface Co atom is strongly reduced by magnitude. At the same time, the calculated MAE of the Co atoms located at the atomic layer 14 is strongly increased by magnitude. The calculated MAE of Cr at the CrAl surface (atomic layer 1) is similar to the one calculated without structural optimization (both are around 0.5 meV/Cr). At the same time, the Cr atoms positioned next to the Co surface now exhibit *positive* MAE. Yet, given a larger (by magnitude) MAE values of the surface Co atoms, and a

larger content of Co per layer (4 vs 2 atoms), the right surface (see figure 1(a)) can be still identified as the one with in-plane magnetization direction.

The most significant difference between the results presented in figures 4 and 5 is that in figure 5 both compressive and tensile strain result in large MCA energies at the 'bulk-like' layers. This results from breaking of the cubic symmetry, i.e. in addition to the surface MCA, there is also a significant contribution from tetragonal distortion induced anisotropy. In particular, while the compressive biaxial strain results in overall positive MAE values of the 'bulk-like' atomic layers (see figures 5(a) and (b)), the tensile strain leads to negative MAE values in the 'bulk-like' layers (see figures 5(e) and (f)). In other words, for c/a > 1 the magnetic moments of the 'bulk-like' layers point in z-direction, while for c/a < 1 these moments are aligned in xy-plane.

4. Discussion and conclusions

The results presented here indicate that CrAl-terminated thin film Co₂CrAl may be very appealing for various spintronic applications, such as in magnetic tunnel junctions. Yet, for practical purposes, one needs to consider a few additional mechanisms not discussed in this work. For example, in multilayer geometry, the surface and interface MCA may have different profiles, due to the overlap of the interface orbitals. Although the role of a substrate may be decisive, these type of ab initio calculations would require much larger cells, and are computationally extremely challenging. In addition, the results reported in this work should be treated as being alloyspecific, i.e. they cannot be generalized to any Co and/or Cr terminated surfaces. Indeed, both perpendicular and in-plane magnetic anisotropies have been reported in the past for thin film cobalt, or cobalt containing alloys. For example, PMA has been reported in ultrathin CoFeB layers used as electrodes in magnetic tunnel junctions [53,54], in thin cobalt film grown on graphene [55], Co films grown on Pt/Ta underlayer [56], etc. At the same time, in-plane magnetic anisotropy was reported e.g. in cobalt thin films deposited on GaAs, Si and glass substrates [57]. A transition from PMA to in-plane anisotropy has been also reported, e.g. in CoFe/MgO/CoFe tunnel junctions, where increasing the Co content in CoFe layer results in out-of-plane to in-plane magnetization transition [58]. These arguments need to be taken into account for potential practical implementations of the presented results.

In addition, based on the presented results, for practical implementations, where PMA is needed (e.g. for hard magnet applications), one should consider substrates, which provide a compressive strain, or good lattice matching with Co₂CrAl, since a large tensile strain may result in a large tetragonal distortion induced anisotropy in non-interfacial layers, comparable with the surface MCA (see figures 5(e) and (f)), and detrimental to PMA. A good candidate could be GaAs (a = 5.650Å) [59], which provides a close lattice matching with Co₂CrAl, with a relatively small compressive strain, and therefore could potentially be used as a substrate for thin-film growth, while maintaining PMA in CrAl-terminated Co₂CrAl. At the same time, in practice, if this material is grown in a thin-film geometry, its thickness is likely to be much larger than 4 unit cells reported in this work. For thicker cells, the effect of atomic relaxations in 'bulk-like' cells is going to be relatively small, and therefore it is plausible to suggest that for realistic implementations (thicker cells) the main results reported in this work are mostly dominated by two physical mechanisms, namely surface MCA, and atomic relaxations at the surface/interface layers.

In thin films, in addition to surface MCA, one needs to take into account the magnetostatic energy (shape anisotropy). In particular, the total anisotropy energy per unit volume, K is given by $K = K_{\rm m} + K_{\rm s}/d$, where $K_{\rm m}$ is the shape anisotropy energy, d is the film thickness, and K_s is the surface MCA energy [23]. For the considered cell, the latter is estimated as $K_s = 0.25$ mJ m⁻² per CrAl surface. Assuming symmetrical CrAl-terminated cell, the MAE contribution to the total anisotropy energy is twice this number, i.e. $K_s =$ 0.5 mJ m⁻². The shape anisotropy energy may be estimated as $K_{\rm m} = -(1/2) \,\mu_0 M^2$, where M is the saturation magnetization [60]. The saturation magnetization of Co₂CrAl is 3.00 $\mu_B/f.u.$ This results in the shape anisotropy energy, $K_{\rm m} = -0.24 \times 10^5 \ {\rm J \ m^{-3}}$. To compare this with the surface MCA energy, one needs to multiply this number by the film thickness. Assuming a 20 nm thin film, one gets $K_{\rm m}d=$ -0.48 mJ m⁻². Thus, it appears that for film thicknesses of 20 nm or less the MCA energy is larger than magnetostatic energy by magnitude, and therefore Co₂CrAl with CrAlterminated surfaces could exhibit PMA. At the same time, for thicker films, the contribution of the shape anisotropy may become decisive, which could result in in-plane magnetization.

Experimental verification of the presented results may be somewhat challenging (to observe PMA, one needs a CrAl-terminated film), but not impractical. In particular, half-metallicity has been experimentally confirmed recently by Jin *et al* in a thin film quaternary Heusler alloy CoFeCrAl

[61], which has a chemical composition similar to Co₂CrAl. We therefore hope that our results will stimulate a further experimental work on this alloy.

In conclusion, we showed from first principles that the full Heusler compound Co2CrAl may exhibit a robust PMA with out-of-plane magnetization orientation, along with halfmetallic electronic structure, at CrAl-terminated surface. At the same time, the Co surface termination not only results in reduced SP due to the emergence of minority-spin surface states at the Fermi level, but also exhibits in-plane magnetization orientation. In addition, for films thicker than 20 nm the contribution from magnetic shape anisotropy may become decisive, resulting in in-plane magnetization orientation. The reported PMA is mainly determined by two physical mechanisms, namely surface MCA and structural relaxation (tetragonal distortion). According to our results, for practical nano-electronics device applications it may be very desirable to grow this material in thin-film geometry with CrAl-termination, preferably under compressive strain or at a good lattice matching with the substrate. We are not aware of any earlier reports of half-metallic thin-film surfaces with PMA, and we therefore hope that our results could stimulate experimental research in this direction.

Acknowledgments

This research is supported by the National Science Foundation (NSF) under Grant Nos. 2003828 and 2003856 via DMR and EPSCoR, and by the Department of Energy (DOE) SBIR sub-award from the Euclid Beamlabs, LLC (Phase I SBIR DE-SC0020564). This work used the Extreme Science and Engineering Discovery Environment (XSEDE), which is supported by National Science Foundation Grant Number ACI-1548562. This work used the XSEDE Regular Memory (Bridges) and Storage (Bridges Pylon) at the Pittsburgh Supercomputing Center (PSC) through allocation TG-DMR180059, and the resources of the Center for Functional Nanomaterials, which is a US DOE Office of Science Facility, and the Scientific Data and Computing Center, a component of the Computational Science Initiative, at Brookhaven National Laboratory (BNL) under Contract No. DE-SC0012704.

ORCID iDs

Parashu Kharel https://orcid.org/0000-0001-7133-0718
Pavel V Lukashev https://orcid.org/0000-0002-2551-5954

References

- [1] Dieny B and Chshiev M 2017 Rev. Mod. Phys. 89 025008
- [2] Wen Z, Sukegawa H, Furubayashi T, Koo J, Inomata K, Mitani S, Hadorn J P, Ohkubo T and Hono K 2014 Adv. Mater. 26 6483
- [3] Nozaki T, Shiota Y, Shiraishi M, Shinjo T and Suzuki Y 2010 Appl. Phys. Lett. 96 022506
- [4] Nakamura K, Shimabukuro R, Fujiwara Y, Akiyama T, Ito T and Freeman A J 2009 Phys. Rev. Lett. 102 187201

- [5] Heinonen O G and Dimitrov D V 2010 J. Appl. Phys. 108 014305
- [6] Zhang J, Lukashev P V, Jaswal S S and Tsymbal E Y 2017 Phys. Rev. B 96 014435
- [7] Mangin S, Ravelosona D, Katine J A, Carey M J, Terris B D and Fullerton E E 2006 *Nat. Mater.* **5** 210
- [8] Boulle O et al 2008 Phys. Rev. Lett. 101 216601
- [9] Yakata S, Kubota H, Suzuki Y, Yakushiji K, Fukushima A, Yuasa S and Ando K 2009 J. Appl. Phys. 105 07D131
- [10] Matsukura F, Tokura Y and Ohno H 2015 *Nat. Nanotechnol.* **10** 209
- [11] Tsymbal E Y 2012 Nat. Mater. 11 12
- [12] Niazi T, Cormier M, Lucot D, Largeau L, Jeudy V, Cibert J and Lemaître A 2013 Appl. Phys. Lett. 102 122403
- [13] Deka A, Rana B, Anami R, Miura K, Takahashi H, Otani Y and Fukuma Y 2020 Phys. Rev. B 101 174405
- [14] Lukashev P V, Horrell N and Sabirianov R F 2012 J. Appl. Phys. 111 07A318
- [15] Staruch M, Gopman D B, Iunin Y L, Shull R D, Cheng S F, Bussmann K and Finkel P 2016 Sci. Rep. 6 37429
- [16] Duan C-G, Velev J P, Sabirianov R F, Zhu Z, Chu J, Jaswal S S and Tsymbal E Y 2008 Phys. Rev. Lett. 101 137201
- [17] Nozaki T et al 2020 APL Mater. 8 011108
- [18] Su Y, Li M, Zhang J, Hong J and You L 2020 J. Magn. Magn. Mater. 505 166758
- [19] Chen W Z, Jiang L N, Yan Z R, Zhu Y, Wan C H and Han X F 2020 Phys. Rev. B 101 144434
- [20] Lukashev P V, Paudel T R, López-Encarnación J M, Adenwalla S, Tsymbal E Y and Velev J P 2012 ACS Nano 6 9745
- [21] Lukashev P V, Burton J D, Jaswal S S and Tsymbal E Y 2012 J. Phys.: Condens. Matter 24 226003
- [22] Wen Z, Sukegawa H, Mitani S and Inomata K 2011 Appl. Phys. Lett. 98 242507
- [23] Takamura Y, Suzuki T, Fujino Y and Nakagawa S 2014 *J. Appl. Phys.* **115** 17C732
- [24] de Groot R A, Mueller F M, Engen P G V and Buschow K H J 1983 Phys. Rev. Lett. 50 2024
- [25] Galanakis I, Dederichs P H and Papanikolaou N 2002 Phys. Rev. B 66 174429
- [26] Picozzi S, Continenza A and Freeman A J 2002 Phys. Rev. B 66 094421
- [27] Balke B, Fecher G H, Winterlik J and Felser C 2007 Appl. Phys. Lett. 90 152504
- [28] Winterlik J et al 2012 Adv. Mater. 24 6283
- [29] Galanakis I 2016 Heusler Alloys (Springer Series in Materials Science vol 222) ed C Felser and A Hirohata (Berlin: Springer)
- [30] Lukashev P et al 2016 Appl. Phys. Lett. 108 141901

- [31] Herran J, Carlile R, Kharel P and Lukashev P V 2019 J. Phys.: Condens. Matter 31 495801
- [32] van Leuken H and de Groot R A 1995 Phys. Rev. Lett. 74 1171
- [33] Buschow K H J and van Engen P G 1981 J. Magn. Magn. Mater. 25 90
- [34] Galanakis I 2002 J. Phys.: Condens. Matter 14 6329
- [35] Galanakis I 2004 J. Phys.: Condens. Matter 16 8007
- [36] Zhang M et al 2004 J. Magn. Magn. Mater. 277 130
- [37] Block T, Carey M J, Gurney B A and Jepsen O 2004 Phys. Rev. B 70 205114
- [38] Kudryavtsev Y V et al 2008 Phys. Rev. B 77 195104
- [39] Jourdan M, Jorge E A, Herbort C, Kallmayer M, Klaer P and Elmers H-J 2009 Appl. Phys. Lett. 95 172504
- [40] Kourov N, Lukoyanov A and Marchenkov V 2013 Fiz. Tverd. Tela 55 2366(original Russian text)
- [41] Kourov N I, Korolev A V, Marchenkov V V, Lukoyanov A V and Belozerova K A 2013 Phys. Solid State 55 977
- [42] Hirohata A, Kurebayashi H, Okamura S, Kikuchi M, Masaki T, Nozaki T, Tezuka N and Inomata K 2005 J. Appl. Phys. 97 103714
- [43] Husmann A and Singh L J 2006 Phys. Rev. B **73** 172417
- [44] Blöchl P E 1994 Phys. Rev. B 50 17953
- [45] Kresse G and Joubert D 1999 Phys. Rev. B **59** 1758
- [46] Perdew J P, Burke K and Ernzerhof M 1996 Phys. Rev. Lett. 77 3865
- [47] Methfessel M and Paxton A T 1989 Phys. Rev. B 40 3616
- [48] 2017 MedeA version-2.22 (San Diego: Materials Design)
- [49] Towns J et al 2014 XSEDE: accelerating scientific discovery Comput. Sci. Eng. 16 62–74
- [50] Yamauchi K and Picozzi S 2010 Phys. Rev. B 81 024110
- [51] Kübler J 2000 Theory of Itinerant Electron Magnetism (New York: Oxford University Press)
- [52] Antropov V, Ke L and Åberg D 2014 Solid State Commun. 194 35
- [53] Ikeda S et al 2010 Nat. Mater. 9 721
- [54] Yakata S, Kubota H, Suzuki Y, Yakushiji K, Fukushima A, Yuasa S and Ando K 2009 J. Appl. Phys. 105 07D131
- [55] Jamali M, Lv Y, Zhao Z and Wang J-P 2014 AIP Adv. 4 107102
- [56] Ootera Y, Shimada T, Kado M, Quinsat M, Morise H, Nakamura S and Kondo T 2015 Appl. Phys. Express 8 113005
- [57] Shukla V, Mukherjee C, Chari R, Rai S, Bindra K S and Banerjee A 2014 J. Magn. Magn. Mater. 370 100
- [58] Zhang J, Franz C, Czerner M and Heiliger C 2014 Phys. Rev. B 90 184409
- [59] Şaşıoğlu E 2009 *Phys. Rev.* B **79** 100406(R)
- [60] Aharoni A 2001 Introduction to the Theory of Ferromagnetism 2nd edn (Oxford: Oxford University Press)
- [61] Jin Y et al 2016 Appl. Phys. Lett. 109 142410